Many-body effects in the photoionization of radon

Mickey Kutzner, Paul Pelley, Lauralea Banks, Richard Robertson, and Lloyd Caesar
Department of Physics, Andrews University, Berrien Springs, Michigan 49104-0380
(Received 5 November 1999; published 8 May 2000)

The total and partial photoionization cross sections, branching ratios, and photoelectron angular-distribution asymmetry parameters have been calculated for atomic radon ($Z=86$) for all subshells from the $6p$ valence shell down to the deep $n=3$ subshells. The relativistic random-phase approximation, the relativistic random-phase approximation modified to include relaxation effects, and the relativistic random-phase approximation modified to include relaxation effects and Auger decay were all used to determine the relative importance of various many-body effects such as interchannel coupling, core relaxation, and Auger decay. Comparisons are made between the various theoretical models and experimental data for the total cross sections. Interchannel coupling among many channels was found to be important in calculations of the total cross sections for most shells, and relaxation effects were found to be substantial for the $n=5$ shell.

PACS number(s): 32.80.Fb

I. INTRODUCTION

Radon is the heaviest of the noble-gas atoms, and thus offers a unique opportunity to study purely atomic photoionization at high Z. In particular, electrons in the deep inner shells of radon have very large effective Z and are thus highly relativistic. It is interesting to evaluate the importance of correlation effects such as interchannel coupling and core relaxation near the photoionization thresholds of deep inner subshells.

Experimental x-ray absorption spectra at particular characteristic wavelengths were reported for radon and many other elements by Henke *et al.* [1]. Binding energies for many of the subshells of radon have been measured by Bearden and Burr [2]. Unfortunately, experimental work on high-Z systems such as radon are limited partly because of the radioactive nature of many such elements. Theoretical work on radon photoionization has included studies using relativistic Dirac-Slater calculations of the $6p$ subshell [3] and the $5d$ subshell [4] and more recently Dirac-Hartree-Fock calculations [5] over a very large range of photon energies. The closed-shell electron structure of the ground state of radon makes photoionization studies within the relativistic random-phase approximation (RRPA) possible. Deshmukh *et al.* [6] calculated photoionization cross sections, angular-distribution asymmetry parameters, and branching ratios for both radon and radium using the RRPA. Their radon calculations included interchannel coupling of the 18 relativistic dipole channels from the $6p$ subshell down to the $5p$ subshell. They found many interesting correlation effects in the photoionization parameters due to interchannel coupling, including correlation-induced Cooper minima in cross sections and dips in the angular-distribution asymmetry parameters.

Core-relaxation effects in calculations of inner-shell photoionization have been of interest for some time [7]. Among the systems for which the inclusion of relaxation effects were found to be crucial are the $4d$ and $3d$ subshells of Xe [8] and Ba [9], the $4f$ subshell of Hg [10], and very recently the $5d$ and $5p$ subshells of Ra [11]. The importance of also including the contribution of overlap integrals between continuum orbitals of the relaxed ion with ground-state orbitals of the neutral initial state was demonstrated for the $1s$ subshell of Ar [12] and Ne [13].

The purpose of this paper is to study the role of many-body effects, in particular interchannel coupling and core relaxation, on the photoionization parameters in the vicinities of various thresholds of atomic radon. The calculations extend from photon energies just above the $6p$ valence-photoionization threshold to energies capable of ejecting electrons from the $n=3$ shell. The calculations were carried out within the framework of the RRPA [14], the relativistic random-phase approximation modified to include relaxation (RRPAR) [9], and the relativistic random-phase approximation modified to include relaxation and Auger decay (RRPARA) [12]. The RRPARA includes overlap integrals between continuum orbitals of the relaxed ion with ground-state orbitals of the neutral initial-state atom. A detailed description of the three theoretical methods can be found elsewhere [9,12,14]. Where possible, we compare the results of theory with experiments [1] to evaluate the merits of the various approximation techniques. The results are reported in Sec. II in a shell-by-shell manner. Section III is a brief discussion of some of the implications of the work.

II. RESULTS

A. The $6p$ subshell

The total photoionization cross section above the valence threshold is shown in Fig. 1 for the RRPA and RRPARA. The RRPAR result is not shown since it is indistinguishable from the RRPARA. Throughout this paper, cross sections are shown as the geometric mean of length and velocity gauge results. The RRPA and RRPARA thresholds are denoted DHF (absolute value of Dirac-Hartree-Fock eigenvalues) and ΔE_{SCF} (absolute value of the difference between total self-consistent energies of the neutral atom and ion), respectively. The experimental data from Henke *et al.* [1] are also shown for comparison. The Dirac-Hartree-Fock calculations of Chantler [5] are shown so that the effects of interchannel coupling may be evaluated. Eighteen relativistic dipole-allowed channels originating from the $6p$ subshells to the $5p$ subshells were included in RRPA-type calculations near the $6p$ threshold. Some of the differences between RRPA-type calculations and DHF [5] appear to be due to threshold dif-

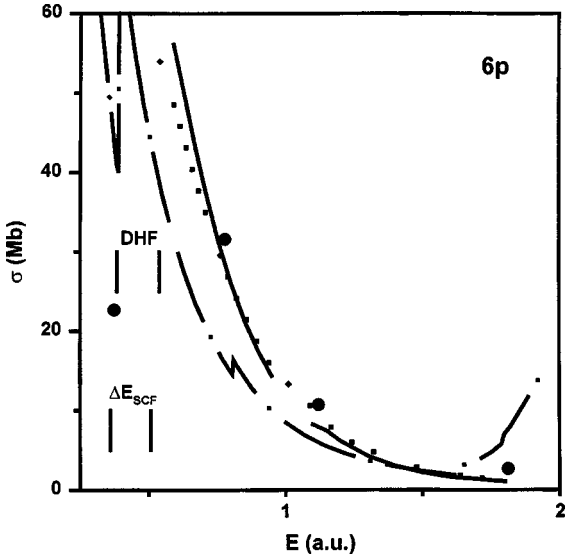

FIG. 1. Photoionization cross sections above the $6p$ threshold of radon. The solid line is the total RRPA cross section; the dotted line is the total RRPARA cross section. RRPAR is not shown but is indistinguishable from the RRPARA. The dot-dashed line is Dirac-Hartree-Fock calculation from Ref. [5]. Solid circles are experimental measurements of total absorption from Ref. [1].

ferences. The RRPA calculations reported here used the absolute value of the DHF eigenvalues as photoionization thresholds, and the RRPARA calculations used the absolute value of the difference between the total self-consistent energies of the neutral atom and ion (ΔE_{SCF}). The computer code of Grant *et al.* [15] was used to obtain these theoretical thresholds. These are not always in agreement with the theoretical thresholds given in Ref. [5] (see Table I). Relaxation effects play only a very minor role for this subshell, and the RRPA appears to give an excellent description of the total photoionization cross section. The inclusion of relaxation as part of the photoelectron potential can actually yield an incorrect result for valence electrons, since relaxation effects in the initial state can also be important and tend to cancel effects due to the relaxation of the final state.

Angular-distribution asymmetry parameters for the $6p_{3/2}$ and $6p_{1/2}$ subshells are shown in Fig. 2 in the RRPA and RRPARA. There is quantitatively little difference between the RRPA and RRPARA calculations near threshold.

Another photoionization parameter of interest is the branching ratio $\gamma \equiv \sigma(6p_{3/2})/\sigma(6p_{1/2})$. Shown in Fig. 3, this parameter varies significantly from the statistical value based on the ratio of occupation numbers of 2 in this region, as reported earlier by Deshmukh *et al.* [6]. The branching ratio falls below the value of 2 because both the $6p_{3/2}$ and $6p_{1/2}$ partial cross sections become smaller with increasing energy, and the $6p_{3/2}$ begins its decline at a lower threshold energy than does the $6p_{1/2}$. Here again, the relaxation effects are subtle.

B. The $5d$ subshell

The total $5d$ photoionization cross section is shown in Fig. 4 in the RRPA and RRPARA along with experimental

TABLE I. Photoionization thresholds (in a.u.) for the various subshells of atomic radon. The second column lists the absolute values of single-particle eigenvalues from a Dirac-Hartree-Fock (DHF) calculation using the code of Ref. [15]. The third column lists the absolute value of the difference between self-consistent-field calculations of total energy of the neutral atom and the ion (ΔE_{SCF}). The fourth column lists theoretical energies from Ref. [5]. The fifth column lists the experimental threshold energies [2]. Threshold energies for the valence subshells are not given in Ref. [2].

Subshell J	DHF	ΔE_{SCF}	Ref. [5]	Exp. [2]
$6p_{3/2}$	0.383 897	0.361 33	0.261 869	
$6p_{1/2}$	0.540 327	0.507 813	0.388 533	
$6s_{1/2}$	1.072 660	1.033 20	0.806 263	0.955
$5d_{5/2}$	2.016 237	1.873 047	1.626 33	1.76
$5d_{3/2}$	2.189 242	2.039 063	1.789 35	1.76
$5p_{3/2}$	5.175 256	4.996 094	4.366 41	4.667
$5p_{1/2}$	6.408 925	6.205 078	5.577 44	6.027
$5s_{1/2}$	8.416 623	8.203 125	7.380 34	7.864
$4f_{7/2}$	8.927 239	8.417 969	7.812 40	8.746
$4f_{5/2}$	9.192 872	8.673 828	8.071 23	8.746
$4d_{5/2}$	20.437 38	19.931 64	19.7342	19.88
$4d_{3/2}$	21.546 44	21.023 44	20.8220	20.82 ± 0.15
$4p_{3/2}$	30.118 73	29.599 61	28.2232	28.2 ± 1.5
$4p_{1/2}$	36.020 71	35.447 27	34.1398	34.1 ± 1.5
$4s_{1/2}$	41.348 32	40.777 34	40.3137	40.31
$3d_{5/2}$	107.7754	106.4570	106.293	106.29 ± 0.11
$3d_{3/2}$	112.5613	111.2266	111.037	111.04 ± 0.11
$3p_{3/2}$	131.7248	130.5176	130.018	130.0 ± 1.4
$3p_{1/2}$	154.9013	153.5957	152.839	152.8 ± 1.4
$3s_{1/2}$	166.9666	165.7129	164.709	164.7

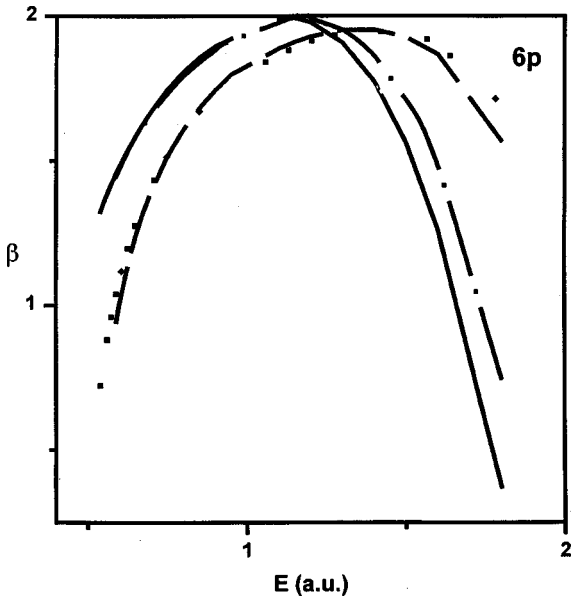

FIG. 2. Photoelectron angular-distribution asymmetry parameter β for $6p$ electrons of radon. The solid and dot-dashed lines are $6p_{3/2}$ in the RRPA and RRPARA, respectively. The dashed and dotted lines are $6p_{1/2}$ in the RRPA and RRPARA, respectively.

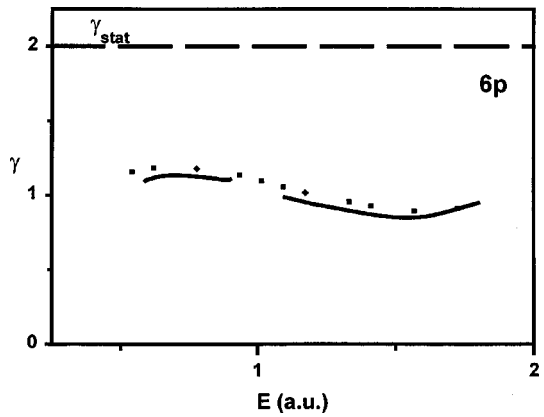

FIG. 3. $6p_{3/2}$:$6p_{1/2}$ branching ratio γ for radon in the RRPA (solid line) and RRPARA (dotted line). The statistical ratio of 2.0 is shown as a dashed line for comparison.

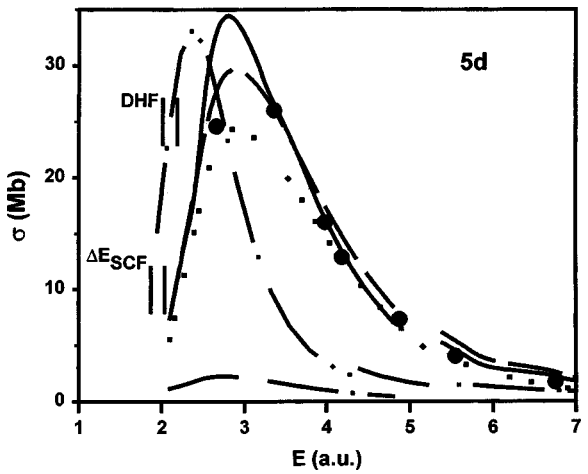

FIG. 4. Photoionization cross sections above the $5d$ threshold of radon. Total cross sections are shown in the RRPA (solid line) and RRPARA (dashed line). The Dirac-Hartree-Fock calculation of Ref. [5] is shown as a double-dot-dashed line. The experimental total cross section from Ref. [1] is shown as solid circles. The partial cross section for direct $5d$ photoionization in the RRPARA is shown as a dotted line and the partial cross section for all other single-excitation channels is shown as a dot-dashed line.

measurements [1] and DHF calculations [5]. The effects of interchannel coupling can be seen by comparing the DHF and RRPA calculations. Aside from a shift of threshold for the two calculations, it appears that the peak in the DHF calculation is sharper and the falloff for energies beyond the peak is steeper than the RRPA result. For this shell, we included 24 dipole-allowed channels from the valence $6p$ channels to channels involving $4f$ electrons. It is interesting to note that for radium ($Z=88$), where the effective Z for $5d$ electrons is approximately two units larger, the RRPA cross section drops monotonically with increasing energy from the threshold. Here, the centripetal barrier causes the cross section to assume a ''giant resonance'' form as noted in the $4d$ cross sections of Xe [8], Ba [9], and the lanthanides [7].

The effect of relaxation is to broaden and lower the peak, redistributing oscillator strength to higher energies. The limited experimental data near threshold is consistent with either the RRPA or RRPARA. At higher energies, beyond the peak, the RRPA calculations are in better agreement with experiment than the RRPARA, which includes relaxation effects. This is to be expected since, at large photoelectron energies, the ion does not have time to relax before the photoelectron is far from the ion.

Also shown in Fig. 4 is the partial cross section for the direct knockout of $5d$ electrons. The experimental data shown [1], however, are only to be compared with the total cross-section calculations. The sum of partial cross sections for all other channels is shown, and it can be seen that interchannel coupling of these weaker channels with the stronger $5d$ channel causes the weak channels to be enhanced. It should also be noted that in the RRPARA the sum of all of the single-excitation channel cross sections is less than the total cross section since the inclusion of overlap integrals reduces the partial cross sections substantially. The reduction represents oscillator strength due to multiple-excitation channels in the ''sudden'' approximation [16].

The angular-distribution asymmetry parameter β is less sensitive than the cross section to relaxation effects since it depends on ratios of matrix elements according to the formulation [14,17]

$$\beta_{n\kappa}(\omega)=\left[\frac{1}{2}\frac{(2j-3)}{2j}|D_{j\to j-1}|^2-\frac{3}{2j}\left(\frac{2j-1}{2(2j+2)}\right)^{1/2}\right.$$
$$\times(D_{j\to j-1}D^*_{j\to j}+\text{c.c.})-\frac{(2j-1)(2j+3)}{2j(2j+2)}|D_{j\to j}|^2$$
$$-\frac{3}{2}\left(\frac{(2j-1)(2j+3)}{2j(2j+2)}\right)^{1/2}(D_{j\to j-1}D^*_{j\to j+1}+\text{c.c.})$$
$$+\frac{1}{2}\frac{(2j+5)}{-(2j+2)}|D_{j\to j+1}|^2+\frac{3}{(2j+2)}\left(\frac{2j+3}{2(2j)}\right)^{1/2}$$
$$\left.\times(D_{j\to j}D^*_{j\to j+1}+\text{c.c.})\right](|D_{j\to j-1}|^2+|D_{j\to j}|^2$$
$$+|D_{j\to j+1}|^2)^{-1}. \quad (1)$$

In Fig. 5, β is shown in the RRPA and RRPARA. The significant changes in the $5d$ cross sections are not seen in the β parameter. This has been noted previously in the case of xenon [8], barium [9], and radium [11]. Branching ratios $\gamma=\sigma(5d_{5/2})/\sigma(5d_{3/2})$ for the RRPA and RRPARA are shown in Fig. 6 along with the statistical ratio of 3/2. Although the RRPA and RRPARA differ somewhat near threshold, the calculations agree with one another within 1 a.u. above threshold.

C. The $5p$ subshell

The $5p$ subshell is interesting because of large spin-orbit effects and substantial interchannel-coupling effects. In Fig. 7, the total cross section in the vicinity of the $5p$ thresholds is shown in the RRPA, RRPARA, DHF [5], and experiment [1]. The RRPA model seems to give an excellent description of the total photoionization in this energy region. The DHF

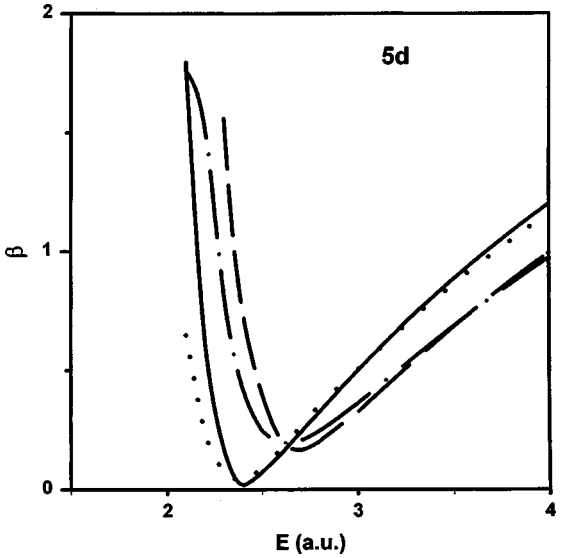

FIG. 5. Photoelectron angular-distribution asymmetry parameter β for $5d$ electrons of radon. The $5d_{5/2}$ is shown as a solid line and dotted line for the RRPA and RRPARA, respectively. The $5d_{3/2}$ is shown as dashed and dot-dashed line for the RRPA and RRPARA, respectively.

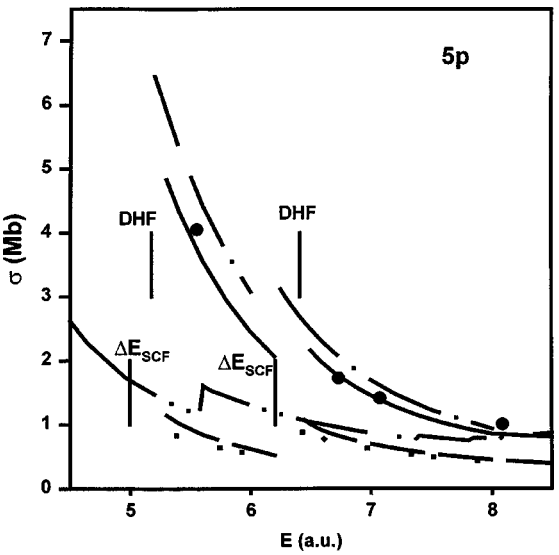

FIG. 7. Photoionization cross sections near the $5p$ thresholds of radon. Total cross sections are shown for RRPA (solid line), RRPARA (dot-dashed line), Dirac-Hartree-Fock from Ref. [5] (double-dot-dashed line), and experiment from Ref. [1] (solid circles). Partial $5d$ and partial $5p$ cross sections in the RRPARA are shown as dashed and dotted lines, respectively.

calculation [5], which does not include interchannel coupling, is well below the experimental measurements. Unlike the case of radium, where the removal of a $5p$ electron caused a radical rearrangement of the $7s$ valence electron orbital, the removal of the $5p$ electron in radon causes only a slight rearrangement of the valence $6p$ orbitals. In the RRPARA calculation, the reduction of the $5p$ single-excitation channel cross sections due to overlap integrals is approximately 10%. The partial cross sections shown in Fig. 7 suggest that the oscillator strength for absorption is approximately evenly divided between the $5p$ channels and the $5d$ channels in this region.

In Fig. 8, the angular-distribution asymmetry parameters β for the $5p$ subshell are presented in the RRPA and RRPARA. The RRPA results for the $5p_{3/2}$ subshell presented here are somewhat lower than those presented by Deshmukh *et al.* [6], presumably because we have included the 26 dipole-allowed channels derived from channels originating from $6p$, $6s$, $5d$, $5p$, $5s$, and $4f$ subshells where Deshmukh *et al.* [6] included the 18 channels originating from $6p$, $6s$, $5d$, and $5p$ subshells. Evidently, the interactions between the $5p$ subshell channels and the $4f$ subshell channels are important. Small relaxation effects are seen for the $5p$ subshell β parameters.

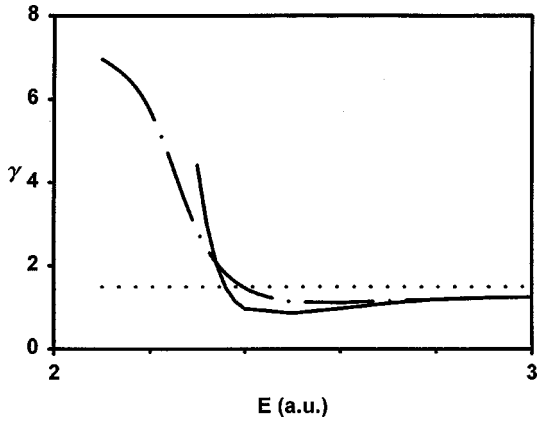

FIG. 6. $5d_{5/2}$:$5d_{3/2}$ branching ratios γ for radon. RRPA is the solid line and RRPARA is the dot-dashed line. The statistical ratio of 3/2 is also shown as a dotted line for comparison purposes.

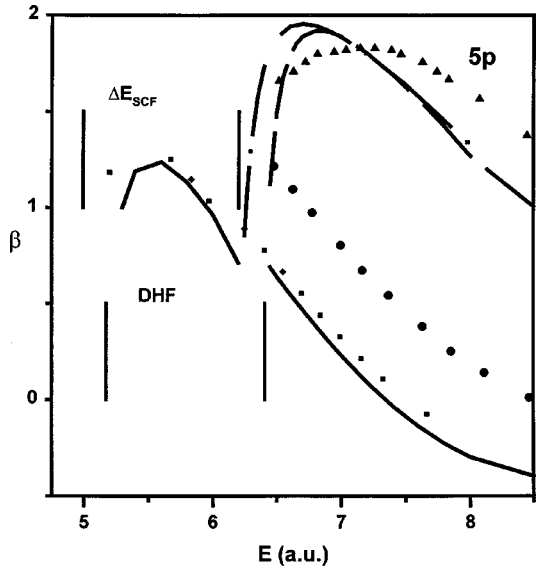

FIG. 8. Photoelectron angular-distribution asymmetry parameters β for $5p$ electrons of radon. For $5p_{3/2}$ electrons, the solid line is RRPA, the dotted line is RRPARA. For $5p_{1/2}$ electrons, the dashed line is RRPA, the dot-dashed line is RRPARA. The 18-channel RRPA calculation of Ref. [6] is shown as solid circles for the $5p_{3/2}$ and solid triangles for the $5p_{1/2}$.

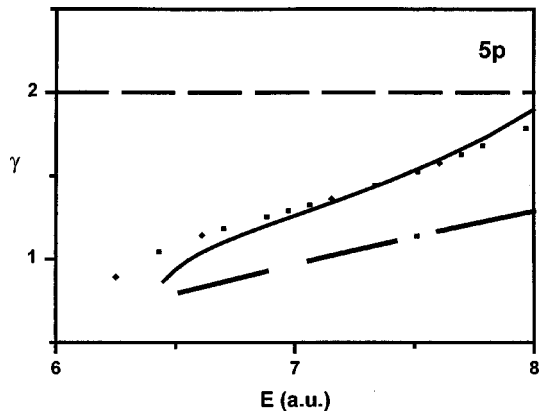

FIG. 9. $5p_{3/2}:5p_{1/2}$ branching ratio γ for radon. The solid line is RRPA and the dotted line is RRPARA. The 18-channel RRPA calculations of Ref. [6] are shown as a dot-dash line. The statistical ratio of 2.0 is indicated as a dashed line.

The branching ratio $\gamma=\sigma(5p_{3/2})/\sigma(5p_{1/2})$ shown in Fig. 9 is somewhat larger than the 18-channel RRPA calculations of Deshmukh *et al.* [6]. Apparently, interchannel coupling between the $5p$ channels and the $5d$ channels is important here.

D. The $4f$ subshell

The $4f$ subshell of radon has had very little theoretical photoionization study prior to the DHF calculations of Chantler [5]. In the case of atomic mercury, it was found that relaxation effects had a large influence on the $4f$ photoionization cross section [10]. For radon, however, the effective Z for $4f$ electrons is considerably stronger than it was for mercury, lessening the importance of relaxation effects. The total photoionization cross sections in the energy region where $n=4$ subshell cross sections dominate the absorption are shown in Fig. 10 in the RRPA, RRPARA, and DHF [5]. The initial rise in the cross section is due to $4f$ photoionization with the centripetal barrier causing a delay in the onset of absorption. The absorption of $4d$ electrons causes the double peaks in the cross section between 18 and 22 a.u. with $4p$ absorption, leading to a slight increase in the cross section near 30 a.u. Interchannel coupling appears to play a role here, reducing the peak of the cross section, and the RRPA agrees well with experiment over a wide energy range. The RRPA-type results shown in Fig. 10 included 30 dipole channels originating from $5d$, $5p$, $4f$, $4d$, $4p$, and $4s$ subshell electrons. Relaxation effects are not large on the total cross section; however, the partial $4f$ cross section (also shown in Fig. 10) is reduced by 14% due to the inclusion of overlap integrals. The $4f$ angular-distribution asymmetry parameters and branching ratios shown in Figs. 11 and 12, respectively, are also not greatly influenced by relaxation effects.

E. The $3d$ subshell

In this extremely deep inner subshell, we might expect most of the many-electron correlation effects to be small compared with the overriding influence of the nucleus. The

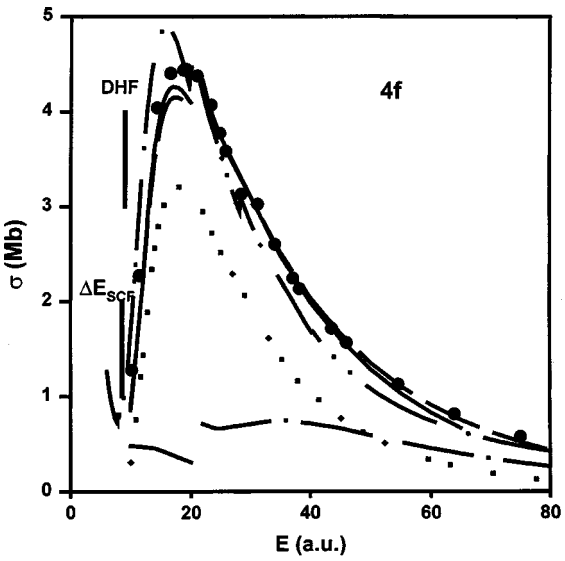

FIG. 10. Photoionization cross sections above the $4f$ threshold of radon. Total cross sections are shown in the RRPA (solid line), RRPARA (dashed line), Dirac-Hartree Fock from Ref. [5] (double-dot-dashed line), and experiment from Ref. [1] (solid circles). The dotted line is the partial photoionization cross section of $4f$ electrons alone in the RRPARA. The dot-dashed line is the sum of the photoionization cross sections from all other single-excitation channels.

total photoionization cross sections above the $3d$ threshold are shown in Fig. 13 for the RRPA, RRPAR, RRPARA, DHF [5], and experiment [1]. The RRPA-type calculations included 32 relativistic dipole-allowed channels, including excitations of $4f$, $4d$, $4p$, $4s$, $3d$, $3p$, and $3s$ electrons. Near threshold, relaxation effects reduce the cross section, as seen in the RRPAR. However, accounting for downward

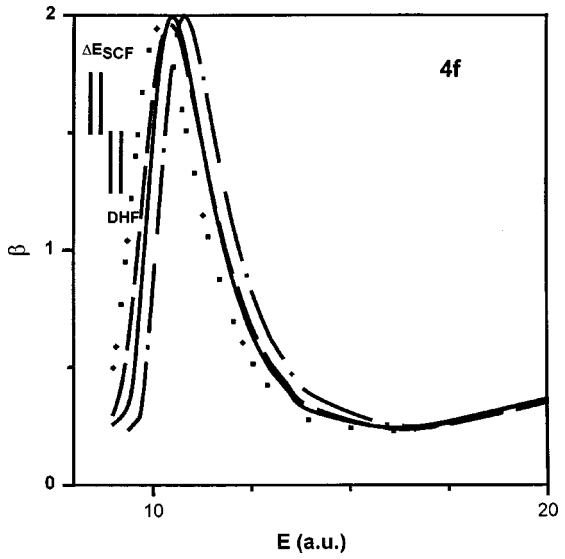

FIG. 11. Photoelectron angular-distribution asymmetry parameters β for $4f$ electrons of radon. For $4f_{7/2}$ electrons results are shown for RRPA (solid line) and RRPARA (dotted line). For $4f_{5/2}$ electrons results are RRPA (dot-dashed line) and RRPARA (dashed line).

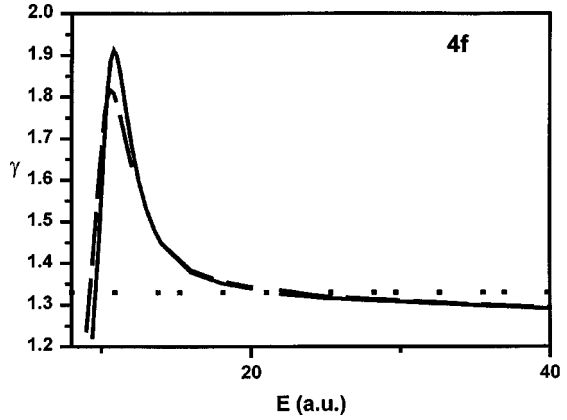

FIG. 12. $4f_{7/2}$:$4f_{5/2}$ branching ratio γ for radon in the RRPA (solid line) and RRPARA (dashed line). The statistical ratio of 4/3 is also shown for comparison.

transitions of $4f$ electrons into the $3d$ vacancy in the RRPARA, nearly restores the total cross section to the RRPA prediction. At high energies, all three RRPA-type models and the DHF calculations [5] are in reasonable agreement with the measured cross section [1] and with each other, signifying that many-body effects are no longer very important and that interactions with the nucleus dominate the process. However, near threshold there is a significant departure between the RRPA-type calculations and the DHF [5], showing that interchannel coupling is still an important effect. Figures 14 and 15 show the angular-distribution asymmetry parameters and the branching ratios for the $3d$ subshell. Some residual effects of relaxation may be noted in the branching ratio.

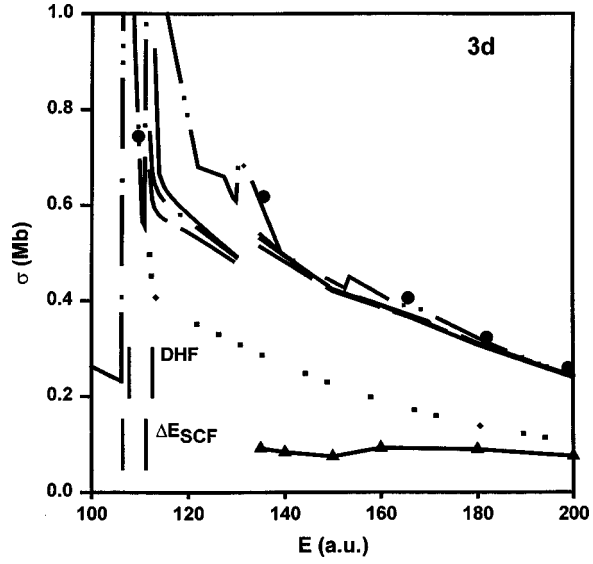

FIG. 13. Photoionization cross sections above the $3d$ thresholds of radon. Total cross sections are shown for RRPA (solid line) RRPAR (dashed line), and RRPARA (dot-dashed line), Dirac-Hartree-Fock (double-dot-dashed line) from Ref. [5], and experiment from Ref. [1] (solid circles). The partial cross section for direct photoionization of $3d$ electrons is shown in the RRPARA as a dotted line. The summed partial cross sections for all other single-excitation channels is shown as a line with solid triangles.

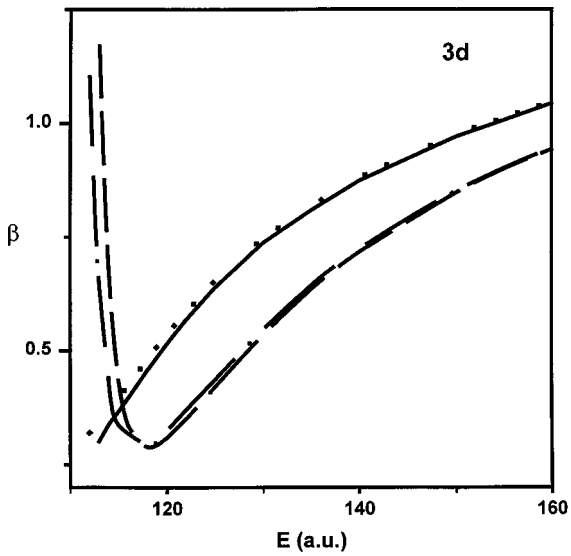

FIG. 14. Photoelectron angular-distribution asymmetry parameter β for $3d$ electrons of radon. For $3d_{5/2}$ electrons, results are shown in the RRPA (solid line) and RRPARA (dotted line). For $3d_{3/2}$ electrons, results are also shown for RRPA (dashed line) and RRPARA (dot-dashed line).

III. CONCLUSION

Interchannel coupling and relaxation effects have been evaluated for photoionization parameters for the various subshells of radon. Differences between RRPA and DHF calculations in the valence $6p$ subshell can probably be explained by differences in threshold energies. The most striking many-body effects are found for photoionization of electrons from the $n=5$ shell, where both interchannel coupling and relaxation effects are notable. Relaxation effects in radon are not as prominent as was seen in radium [11] because of the absence of the sensitive $7s$ valence-shell electrons.

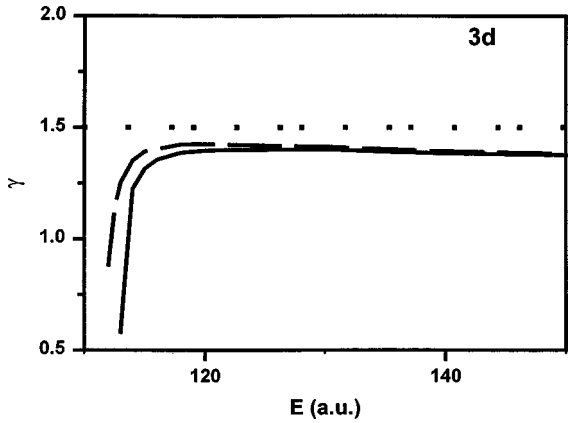

FIG. 15. $3d_{5/2}$:$3d_{3/2}$ branching ratio γ for radon. RRPA is shown by a solid line and RRPARA is shown by the dashed line. The statistical ratio of 3/2 is shown as a dotted line.

Interchannel-coupling effects are noted for the $4f$ subshell cross sections, but relaxation effects are small. For the very deep $n=3$ subshell, notable differences persist near threshold between models that include interchannel coupling and the one-electron model [5].

It is hoped that the theoretical work presented here will stimulate additional experimental work on radon and other high-Z atoms. In particular, the new synchrotron light sources could be used to yield absorption spectra with more detail near each of the thresholds where many-body effects are important. Detail in the resonance regions below thresholds could be measured and analyzed using the RRPA in conjunction with relativistic multichannel quantum-defect theory to determine the effectiveness of resonance models at high Z. Also, photoelectron spectroscopy could be used to determine partial cross sections for single- and multiple-excitation channels.

ACKNOWLEDGMENTS

The authors wish to thank V. Radojević for use of the RRPAR code and Walter Johnson for use of the RRPA code. We also acknowledge Stephen E. Vance and Quinn Shamblin for their role in the development of the RRPARA model. This work has been supported in part by Grant No. PHY-9707183 of the National Science Foundation and by the Office of Scholarly Research of Andrews University.

[1] B. L. Henke, E. M. Gullikson, and J. C. Davis, At. Data Nucl. Data Tables **54**, 181 (1993).
[2] J. A. Bearden and A. F. Burr, Rev. Mod. Phys. **39**, 125 (1967).
[3] S. T. Manson, C. J. Lee, R. H. Pratt, I. B. Goldberg, B. R. Tambe, and A. Ron, Phys. Rev. A **28**, 2885 (1983).
[4] B. R. Tambe and S. T. Manson, Phys. Rev. A **30**, 256 (1984).
[5] C. T. Chantler, J. Phys. Chem. Ref. Data **24**, 71 (1995).
[6] P. C. Deshmukh, V. Radojević, and S. T. Manson, Phys. Rev. A **45**, 6339 (1992).
[7] M. Ya. Amusia, in *Atomic Photoeffect*, edited by P. G. Burke and H. Kleinpoppen (Plenum, New York, 1990).
[8] Z. Altun, M. Kutzner, and H. P. Kelly, Phys. Rev. A **37**, 4671 (1988).
[9] V. Radojević, M. Kutzner, and H. P. Kelly, Phys. Rev. A **40**, 727 (1989); M. Kutzner, D. Winn, and S. Mattingly, *ibid.* **48**, 404 (1993).
[10] M. Kutzner, C. Tidwell, S. E. Vance, and V. Radojević, Phys. Rev. A **49**, 300 (1994).
[11] M. Kutzner, P. Pelley, L. Banks, and R. Robertson, Phys. Rev. A **61**, 022717 (2000).
[12] M. Kutzner, Q. Shamblin, S. E. Vance, and D. Winn, Phys. Rev. A **55**, 248 (1997).
[13] M. Kutzner and M. Rose, J. Phys. B **32**, 123 (1999).
[14] W. R. Johnson and C. D. Lin, Phys. Rev. A **20**, 964 (1979); W. R. Johnson, C. D. Lin, K. T. Cheng, and C. M. Lee, Phys. Scr. **21**, 403 (1980).
[15] I. P. Grant, B. J. McKenzie, P. H. Norrington, D. F. Mayers, and N. C. Pyper, Comput. Phys. Commun. **21**, 207 (1980).
[16] T. Åberg, *Photoionization and Other Probes of Many-Electron Interactions* (Plenum, New York, 1976).
[17] T. E. H. Walker and J. T. Waber, J. Phys. B **7**, 674 (1974).